45th AIAA/ASME/SAE/ASEE Joint Propulsion Conference & Exhibit
2 - 5 August 2009, Denver, Colorado

AIAA 2009-5361

Two-dimensional plasma acceleration in a divergent magnetic nozzle

E. Ahedo * and M. Merino †

E.T.S. Ingenieros Aeronáuticos, Universidad Politécnica de Madrid, 28040 Madrid, Spain

The acceleration of a current-free plasma in a divergent magnetic nozzle with fully magnetically guided electrons is discussed. Ion momentum is gained from the electron thermal pressure, via the electrostatic self-field. Except for very large magnetic fields, ion magnetization is weak and ion streamlines deviate from magnetic streamlines. As a consequence the local ambipolar condition does not hold, and local electric currents are formed. Azimuthal ion and electron currents are evaluated. The acceleration efficiency is computed.

I. Introduction

A divergent magnetic nozzle, created by a longitudinal magnetic field is being used as an acceleration mechanism of a magnetized plasma in different propulsion devices such as the applied-field magnetoplasmadynamic (MPD) thruster,[1] the helicon thruster,[2] the VASIMR,[3] and the diverging cusped field thruster (DCFT).[4] There is a clear analogy between the dynamics of a magnetized plasma in a magnetic nozzle and a neutral gas in a solid (deLaval) nozzle: the plasma flow is tied to the magnetic streamlines and a regular sonic transition occurs at the magnetic throat, i.e. the cross-section where the magnetic field is maximum.[5] However, plasma physics in a magnetic nozzle appear to be more complex than gas dynamics in a solid nozzle. For instance: there are several possible sources of plasma 'internal' energy; Lorentz forces compete with thermal pressure; the plasma can be put into rotation; self-magnetic fields can be created; the response changes with plasma collisionality and ion magnetization. In addition, the plasma must detach downstream from the turning magnetic lines in order to achieve the desired axial thrust.[6–9]

Analytical studies of subsonic-to-supersonic plasma acceleration in a magnetic nozzle are mostly reduced to 1D models. The simplest model assumes an isothermal plasma with no azimuthal fluxes;[5] the isothermal condition seems more adequate for a confined electron population. Ahedo and Martínez-Sánchez have extended this basic nozzle model to plasmas with two electron populations of disparate temperatures, in order to show the formation of profile steepening and, in some cases, a weak double layer.[10] Evidence of these structures has been observed in helicon thrusters.[11]

This work presents a 2D (axisymmetric) model of the supersonic acceleration of a collisionless plasma in a divergent magnetic nozzle, aimed at discussing mainly the physical aspects absent from the 1D model. The analyses of both the *upstream* subsonic region (in a convergent nozzle or inside a solid device), where the plasma is generated and heated, and the *downstream* detachment region are out of the scope of the present work. 2D simulations of supersonic plasmas in magnetic nozzles have been carried out by Winglee et al.[12] for a helicon thruster, using a multifluid model and considering induced magnetic fields, and by Mikellides et al.[13] for a fusion propulsion system.

*Professor; AIAA member; e-mail: eduardo.ahedo@upm.es.
†Student.

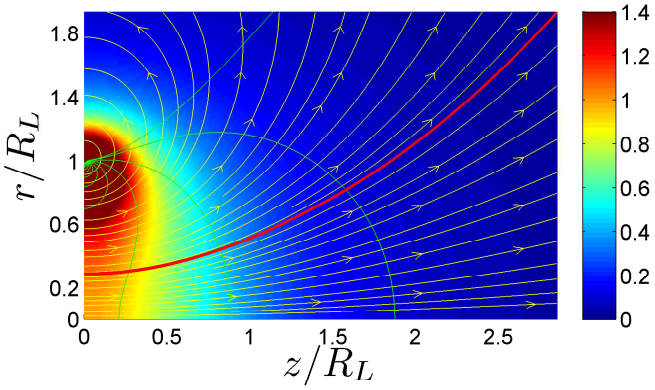

Figure 1. Magnetic streamlines and magnetic strength (in color, arbitrary units) for a circular ring of radius R_L. The red line corresponds to the boundary V of the plasma jet in the nozzle used in the simulations.

II. Model formulation

A collisionless plasma is flowing in a guiding longitudinal magnetic field, $\boldsymbol{B} = B_r\mathbf{1}_r + B_z\mathbf{1}_z$. The cylindrical and magnetic reference frames are $\{\mathbf{1}_z, \mathbf{1}_r, \mathbf{1}_\theta\}$ and $\{\boldsymbol{b}, \mathbf{1}_\perp, \mathbf{1}_\theta\}$, with

$$\boldsymbol{b} = \boldsymbol{B}/B = \cos\alpha\mathbf{1}_z + \sin\alpha\mathbf{1}_r, \quad \mathbf{1}_\perp = -\sin\alpha\mathbf{1}_z + \cos\alpha\mathbf{1}_r.$$

The applied magnetic field is solenoidal, irrotational, and has $B_\theta = 0$. Then, there exists a magnetic streamfunction $\psi(r,z)$ satisfying

$$\nabla\psi = rB\mathbf{1}_\perp : \quad rB_r = -\partial\psi/\partial z, \quad rB_z = \partial\psi/\partial r. \tag{1}$$

We are interested in plasma acceleration in a divergent magnetic field. Results here will be presented for the magnetic field created by a current ring placed at $z = 0$ and of radius R_L. Then, the magnetic streamfunction is

$$\psi(r,z) = \frac{2B_0R_L^2r}{\pi}\cdot\frac{\left(2-k^2\right)\mathbf{K}\left(k^2\right) - 2\mathbf{E}\left(k^2\right)}{k^2\sqrt{\left(R_L+r\right)^2+z^2}}, \tag{2}$$

with

$$k^2 = \frac{4R_Lr}{(R_L+r)^2+z^2},$$

$B_0 = B_z(0,0)$, and $\mathbf{K}\left(k^2\right)$ and $\mathbf{E}\left(k^2\right)$ the complete elliptic integrals of first and second kind, respectively.[14] The magnetic field components are

$$B_r(r,z) = -\frac{B_0R_Lz}{\pi r}\cdot\frac{1}{\sqrt{\left(R_L+r\right)^2+z^2}}\left(\mathbf{K}\left(k^2\right) - \frac{R_L^2+r^2+z^2}{\left(R_L-r\right)^2+z^2}\mathbf{E}\left(k^2\right)\right), \tag{3}$$

$$B_z(r,z) = \frac{B_0R_L}{\pi}\cdot\frac{1}{\sqrt{\left(R_L+r\right)^2+z^2}}\left(\mathbf{K}\left(k^2\right) + \frac{R_L^2-r^2-z^2}{\left(R_L-r\right)^2+z^2}\mathbf{E}\left(k^2\right)\right), \tag{4}$$

Figure 1 plots this magnetic topology.

A. Plasma equations

The collisionless plasma is injected sonically at the nozzle throat, at $z = 0$, and is accelerated in the diverging nozzle. Plasma quasineutrality holds (i.e. $n_e = n_i = n$), axisymmetry applies, and electric currents in the plasma are assumed small enough to neglect the induced magnetic field. Electron inertia effects are disregarded (i.e. $m_e/m_i \to 0$) and the magnetic field is strong enough to guide magnetically electrons; thus electron motion is restricted to magnetic streamsurfaces. With respect to (singly-charged) ions, different magnetization strengths will be considered. A steady-state, axisymmetric (i.e. $\partial/\partial\theta = 0$) model is proposed. For vectorial quantities, such as the ion velocity, $\boldsymbol{u}_i$, it will be convenient to distinguish the meridional (or longitudinal) vectorial component with a tilde; e.g. $\tilde{\boldsymbol{u}}_i = \boldsymbol{u}_i - u_{\theta i}\mathbf{1}_\theta$, etcetera.

The ion continuity equation is

$$\nabla \cdot n\boldsymbol{u}_i = \nabla \cdot n\tilde{\boldsymbol{u}}_i = 0. \tag{5}$$

Then, $\tilde{\boldsymbol{u}}_i$ admits a streamfunction ψ_i, which satisfies

$$rnu_{ri} = -\partial\psi_i/\partial z, \quad rnu_{zi} = \partial\psi_i/\partial r. \tag{6}$$

The ion momentum equations can be expressed as

$$m_i\tilde{\boldsymbol{u}}_i \cdot \nabla u_{\theta i} = e(\tilde{\boldsymbol{u}}_i \times \boldsymbol{B}) \cdot \mathbf{1}_\theta - m_i u_{ri}u_{\theta i}/r, \tag{7}$$

$$m_i\tilde{\boldsymbol{u}}_i \cdot \nabla\tilde{\boldsymbol{u}}_i = -e\nabla\phi + eu_{\theta i}\mathbf{1}_\theta \times \boldsymbol{B} + \mathbf{1}_r m_i u_{\theta i}^2/r, \tag{8}$$

where $\tilde{\boldsymbol{u}}_i \cdot \nabla$ is the derivative along the meridian-projected streamlines. Ion pressure has been neglected based on the facts that it is smaller than (i) the dynamic ion pressure, for a supersonic flow, and (ii) the electron pressure, in many applications. From Eq. (7) we obtain the conservation of the ion axial angular momentum along each ion streamline,

$$rm_i u_{\theta i} + e\psi = D_i(\psi_i). \tag{9}$$

Then, Eq. (8) becomes

$$m_i\tilde{\boldsymbol{u}}_{\boldsymbol{i}} \cdot \nabla\tilde{\boldsymbol{u}}_i = -\nabla\left(e\phi + m_i u_{\theta i}^2/2\right) + (u_{\theta i}/r)\nabla D_i(\psi_i). \tag{10}$$

Observe that Hooper[7] uses Eq. (10), but misses the last term on the right. Therefore, his model is correct only for plasmas having a uniform axial angular momentum, i.e $D_i(\psi_i) = \text{const}$.

Except for the small electron current neutralizing the ion current, electrons are mostly confined. Then, individual electrons travel back-and-forth along the magnetic lines, suffering occasional collisions that tend to thermalize them. The strongly-magnetized electron flow has $\tilde{\boldsymbol{u}}_e = u_{\parallel e}\boldsymbol{b}$, with $\tilde{u}_e \sim \tilde{u}_i \ll \sqrt{T_e/m_e}$. Then, the continuity equation and $\nabla \cdot \boldsymbol{B} = 0$ yield a conservation law for the parallel electron flux,

$$nu_{\parallel e}/B = G_e(\psi), \tag{11}$$

with $G_e(\psi)$ the electron-to-magnetic flux ratio. Therefore, magnetic streamsurfaces are electron streamsurfaces. However, if $u_{\theta e} \neq 0$, electron streamlines are helicoidal and do not coincide with magnetic streamlines. The electron momentum equation leads to

$$T_e \ln n - e\phi = H_e(\psi), \tag{12}$$

$$u_{\theta e} = -\frac{1}{eB}\frac{\partial H_e}{\partial \mathbf{1}_\perp} = -\frac{r}{e}\frac{dH_e}{d\psi}, \tag{13}$$

where, $T_e \ln n$ is the (specific) enthalpy of the electron gas, and $H_e(\psi)$ is the total (specific) enthalpy. Both $G_e(\psi)$ and $H_e(\psi)$ are given by upstream conditions. In each streamsurface, Eq. (12) can be interpreted as either the conservation of total (specific) enthalphy or the Maxwell-Boltzmann equilibrium. Equation (13) states that the azimuthal velocity is an $E \times B$ drift, where $e^{-1}\partial H_e/\partial \mathbf{1}_\perp$ takes the role of a generalized electric field. Observe that since the ratio $u_{\theta e}/r$ remains constant in each streamsurface, if the electron Hall current is zero at the entrance, it will remain zero in the whole nozzle.

magnetic field at entrance, B_0	1000G
plasma density at entrance, n_0	$10^{18}\mathrm{m}^{-3}$
electron temperature, T_e	10eV
thermal velocity, c_e	$1.3 \cdot 10^6\mathrm{m/s}$
sound velocity, c_s	$4.9 \cdot 10^3\mathrm{m/s}$
ion current density, j_i	$800\mathrm{A/m}^2$
ion current, I_i	0.25A
mass flow, $\dot{m}_i$	0.1mg/s
nozzle throat radius, R	$1 \cdot 10^{-2}\mathrm{m}$
Debye length, λ_d	$2.4 \cdot 10^{-5}\mathrm{m}$
electron Larmor radius, l_e	$7.5 \cdot 10^{-5}\mathrm{m}$
ion Larmor radius, l_i	$2.0 \cdot 10^{-2}\mathrm{m}$
electron gyrofrequency, ω_{ce}	$1.8 \cdot 10^{10}\mathrm{s}^{-1}$
lower-hybrid frequency, ω_{lh}	$6.5 \cdot 10^7\mathrm{s}^{-1}$
radial transit frequency, c_s/R	$4.9 \cdot 10^5\mathrm{s}^{-1}$
ion gyrofrequency, Ω_i	$2.4 \cdot 10^5\mathrm{s}^{-1}$

Table 1. Typical parameters at the nozzle throat for a small plasma source.

Substituting the electric potential ϕ from Eq. (12), Eqs. (5) and (7) become a set of three differential equations for n, u_{zi}, and u_{ri}, that are integrated with the method of characteristics.[15] The three families of characteristic curves are the ion streamlines and the pair of Mach lines. The rest of plasma variables (ϕ, $u_{\theta i}$, $u_{\theta e}$, $u_{\parallel e}$) are determined from algebraic conservation equations. An important magnitude is the electric current density,

$$\boldsymbol{j} \equiv \tilde{\boldsymbol{j}} + j_\theta \mathbf{1}_\theta = \boldsymbol{j}_i - \boldsymbol{j}_e, \tag{14}$$

with $\boldsymbol{j}_i = en\boldsymbol{u}_i$ and $\boldsymbol{j}_e = en\boldsymbol{u}_e$ the ion and electron current densities (notice the sign used for j_e).

Let A: $z = 0,\ 0 \le r \le R$ be the 'entrance' section for the plasma jet in our model, with R smaller than R_L, the radius of the current ring. Let V: $r = R_V(z)$ be the tube containing the whole plasma jet, with $R_V(z)$ defined implicitly by the magnetic streamsurface $\psi(R_V(z), z) = \psi(R, 0)$. Although ion streamsurfaces are not going to coincide with the electron streamsurfaces, plasma quasineutrality assures that the external magnetic streamsurface V is an ion streamsurface too. Therefore, the tube V is the magnetic nozzle for the ion flow too.

Simulations here are presented for the simplest case of a plasma jet that, at the entrance, is uniform, current-free, with no rotation and no Hall current. Thus, the entrance conditions are

$$\boldsymbol{u}_i(r, 0) = (0, 0, c_s M_0), \tag{15}$$

$$\boldsymbol{u}_e(r, 0) = (0, 0, c_s M_0), \tag{16}$$

$$n(r, 0) = n_0, \quad \phi(r, 0) = 0 \tag{17}$$

with $c_s = \sqrt{T_e/m_i}$ the sound velocity and $M_0 \ge 1$ the plasma Mach number at the entrance. The entrance conditions determine the ion streamfunction at the entrance, $\psi_i(r, 0)$, and functions $D_i(\psi_i)$, $H_e(\psi)$, and $G_e(\psi)$. In particular, one has $H_e(\psi) = 0$ and, from Eq. (13), the electron Hall current is zero in the whole nozzle.

Magnitudes are non-dimensionalized with the magnetic field B_0, the energy T_e, the velocity c_s, the length R, the density n_0, the current density $j_0 = en_0c_s$, and so on. Dimensionless variables are expressed with a hat, e.g. $\hat{u}_z = u_z/c_s$. Since the plasma is isothermal $\hat{u}_i$ is the Mach number M. The integration runs from $z = 0$ to any radial section located before the turning point $dr/dz|_V \to \infty$ of the magnetic tube V. The

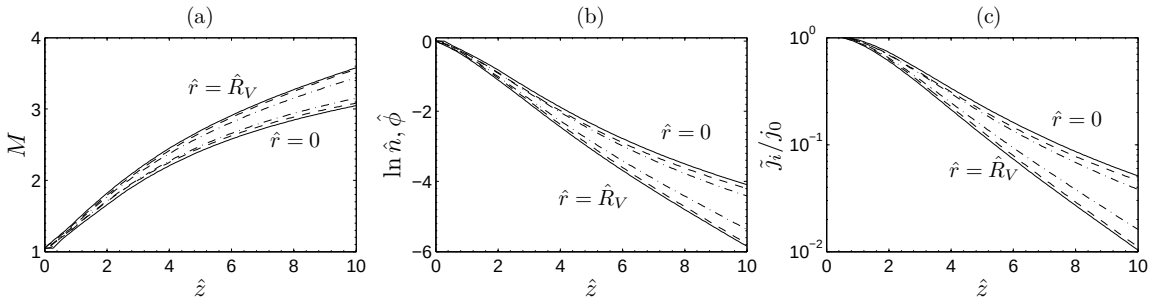

Figure 2. Axial evolution of plasma magnitudes at the two boundary streamlines, $r = 0$ and $r = R_V(z)$, for three magnetization strengths: $\hat{\Omega}_{i0}$ =0.1(solid), 10(dashed), and 100(dash-and-dot).

dimensionless parameters of the problem are

$$\frac{R}{R_L}, \qquad \hat{\Omega}_{i0} = \frac{eB_0R}{m_ic_s} \equiv \frac{R}{\ell_{i0}}, \tag{18}$$

that is the divergence rate of the plasma-filled tube V and the ion magnetization parameter, respectively, with ℓ_{i0} the ion gyroradius at $(z, r) = (0, 0)$. A third parameter is M_0, but, unless otherwise is stated, simulations are run for $M_0 = 1.05$. The method of characteristics does not admit to take $M_0 = 1$, but it has been checked that solutions are not strongly sensitive to small values of $M_0 - 1$. Just for reference, Table 1 gives typical magnitudes for a plasma generated in a small helicon source.

B. Propulsion parameters

The flow of a generic ion magnitude, say χ, across a $z =$ const section is defined as

$$\langle \chi \rangle (z) = 2\pi \int_0^{R_V(z)} drrnu_{zi}\chi. \tag{19}$$

The mass flow, $\dot{m}_i = \langle m_i \rangle$, and the ion current, $I_i = \langle e \rangle$, are constant along the nozzle. Since the longitudinal current density is zero at the entrance, $\tilde{\boldsymbol{j}}_A = \mathbf{0}$, the plasma is current-free globally, $I(z) = 0$. However, it will turn out that $\tilde{\boldsymbol{j}}(r, z) \neq \mathbf{0}$, in general, invalidating the local ambipolarity condition invoked by Hooper.

The flow of axial momentum, axial energy, and total energy correspond to $F_z = \langle m_i u_{zi} \rangle$, $P_z = \langle m_i u_{zi}^2/2 \rangle$, and $P = \langle m_i u_i^2/2 \rangle$. The efficiency of the ion acceleration process in the divergent nozzle is measured by

$$\eta_{noz} = \frac{F_z^2}{2\dot{m}_i P}. \tag{20}$$

The ratio $F_z^2/(2\dot{m}_i P_z)$ measures the radial inhomogeneity on the profiles of the axial flux nu_{zi}.

III. Results

Simulations are presented for a single nozzle with a relatively high divergence rate ($R/R_L = 0.3$) and three ion magnetization strengths: $\hat{\Omega}_{i0} = 0.1$, 10, and 100. For the case of Table 1, this range of $\hat{\Omega}_{i0}$ corresponds to $0.02T < B_0 < 20T$. Although $\hat{\Omega}_{i0} \leq O(1)$ covers sufficiently present and foreseen applications, the range has been extended until 100 in order to show when strong ion magnetization is encountered. The turning point of the tube V for the nozzle is at $(r, z) \approx (22, 16)$ and the integration here is stopped at $z_F = 10$.

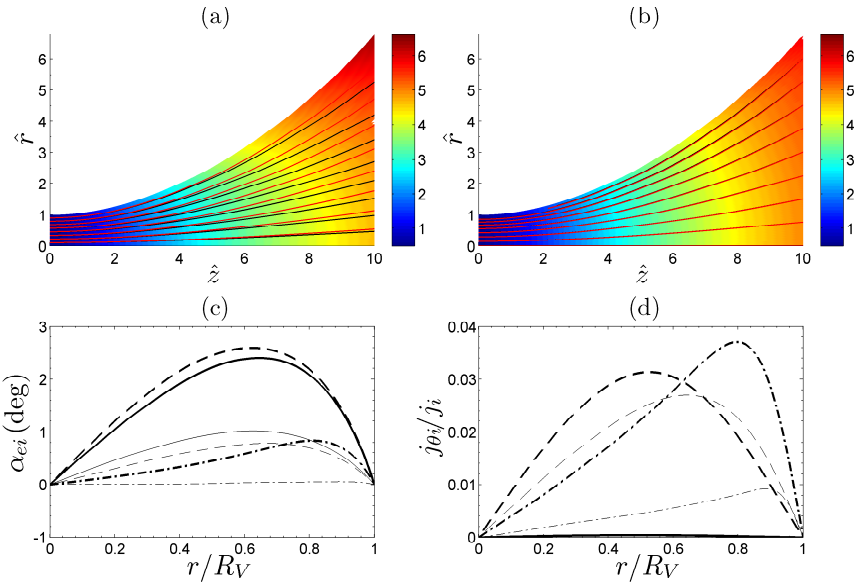

Figure 3. (a)-(b) Ion(black) and electron/magnetic(red) streamlines in the meridional plane for $\hat{\Omega}_{i0} = 0.1$(a) and 100 (b); the color 2D map plots the ion velocity $\hat{u}_i$. (c) Misalignment angle between ion and electron streamlines and (d) relative azimuthal ion current, at z/R =5(thin lines) and 10 (thick lines) for $\hat{\Omega}_{i0}$ =0.1(solid), 10(dashed), and 100(dash-and-dot).

Figures 2(a)-2(c) show the downstream evolution of the main fluid variables at the two 'boundary' streamlines, $r = 0$ and $r = R_V(z)$. The differences between the values at the two streamlines indicate the radial inhomogeneity developed by the plasma jet as it moves downstream. In spite of that inhomogeneity, it is seen that a simple, r-averaged 1D model still provides a fair approximation of the axial evolution of M, ϕ and n, according to $(M^2 - 1)/2 \approx -\hat{\phi} \approx -\ln \hat{n}$. The decrease of the ion density current $\tilde{j}_i$ is due to the area expansion. Contrary to an adiabatic gas, where the sound speed decreases along the nozzle and M quickly becomes hipersonic, $M = \hat{u}_{zi}$ increases slowly in this isothermal plasma. Also, electron pressure and enthalpy are more persistent; in particular, the enthalpy has a logarithmic dependence and does not go to zero.

We turn now to effects and variables not covered by the simple 1D model. The first one is the ion magnetization strength. Figure 3(a) shows the (projection of the) ion and electron (i.e. magnetic) streamlines in the meridional plane for $\hat{\Omega}_{i0} = 0.1$. Because of their low magnetization, ions do not follow the magnetic streamlines, leading to a non-zero electric density current, $\tilde{\boldsymbol{j}} \neq \mathbf{0}$, except at the boundary streamlines. On the contrary, for $\hat{\Omega}_{i0} = 100$, Fig. 3(b), ions are magnetized and almost follow the magnetic streamlines; however we will still find that $\tilde{\boldsymbol{j}} \neq \mathbf{0}$. The case $\hat{\Omega}_{i0} = 10$ is closer to the low magnetization case, so in practical applications ions are not expected to follow closely the magnetic streamlines. The misalignment angle between ion and electron/magnetic streamsurfaces, α_{ei}, is plotted in Fig. 3(c). It is zero at the two boundary lines (as prescribed), it is maximum at an intermediate radius and increases downstream but reaches very modest values. The magnetic misalignment of the ions causes an ion rotation, $u_{\theta i}$, and an azimuthal ion current, shown in Fig. 3(d). This azimuthal current is always small and it is not much affected by ion magnetization because the increase of $\hat{\Omega}_{i0}$ is partially compensated by the decrease of the misalignment angle α_{ei}.

Figure 4 presents one of the most interesting findings of the 2D model: the development of large electric current densities, $\tilde{\boldsymbol{j}}$, despite of the plasma being current-free globally, that is $I(z) = \int_o^{R_v} dr \tilde{j}_z = 0$. Figure 4(a) plots radial profiles of the ratio j_z/j_i, showing that $j_z = j_{zi} - j_{ze} > 0$ in the central part of the jet and

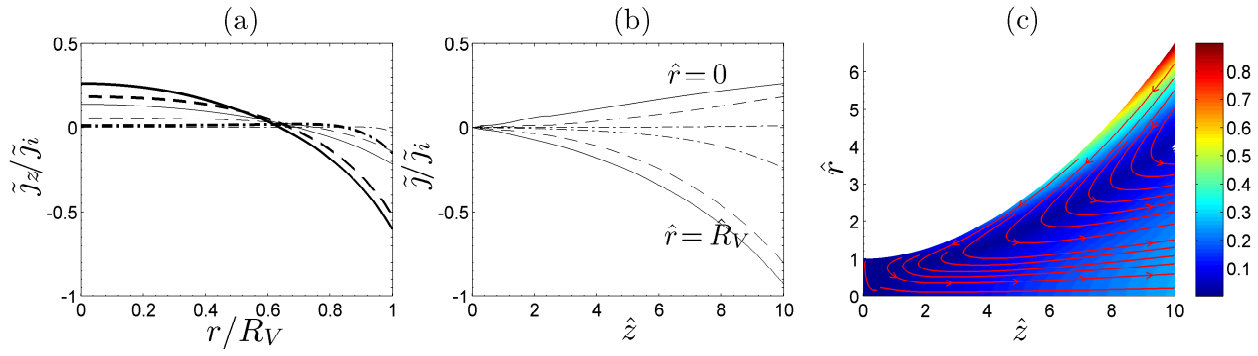

Figure 4. (a) Relative electric current along z for same conditions than Figs.3(c) and 3(d). (b) Relative electric-current for same conditions than Fig. 2. (c) Lines of electric current density and (in color) $|j|/j_i$ for $\hat{\Omega}_{i0} = 0.1$.

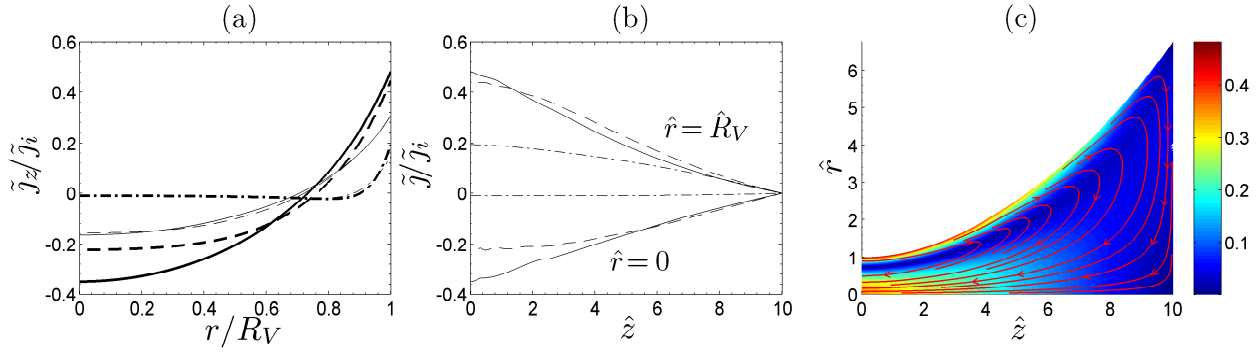

Figure 5. Same than Fig. 4, but imposing $\tilde{j} = 0$ at the end section $z_F = 10$.

$j_{zi} - j_{ze} < 0$ near the external border. Figure 4(b) plots the axial evolution of the relative electric current density, $\tilde{j}/\tilde{j}_i$, at the central and external streamlines, when $\tilde{j}$ and $\tilde{j}_i$ are aligned. Figure 4(c) shows a colored 2D map of $\tilde{j}/\tilde{j}_i$ and the electric current lines. As the misalignment angle between electron and ion flux tubes increases downstream, the ratio $\tilde{j}/\tilde{j}_i$ increases steadily and becomes of order one. For weak ion magnetization [i.e. $\hat{\Omega}_{i0} \leq O(1)$] and $z/R \sim 10$, the electron current is twice the ion current at the jet external border, whereas $\tilde{j}_i \sim 1.2\tilde{j}_e$ at the jet central part. Only for the less realistic case of strong ion magnetization, the electric current density is small compared to the species current densities. The behavior of $\tilde{j}$ also shows that the ion jet is more focused than the 'electron jet', a fact that is positive for ion acceleration and possibly for detachment.

It is worth to observe that the development of large electric currents is a consequence of the modest streamline misalignment. If the misalignment α_{ei} is neglected, so that $\tilde{\boldsymbol{j}}_i$ and $\tilde{\boldsymbol{j}}_e$ are assumed parallel, then equations $\nabla \cdot \tilde{\boldsymbol{j}}_i = 0$, $\nabla \cdot \tilde{\boldsymbol{j}}_e = 0$, and $\tilde{\boldsymbol{j}}_A = \boldsymbol{0}$ lead to $\tilde{j}_e = \tilde{j}_i$ anywhere. Finally, in order to confirm that the development of local electric currents in the expanding jet is not related mainly to the boundary conditions, we have modified these, setting that $\tilde{\boldsymbol{j}} = \boldsymbol{0}$ at the final section $z = z_F$ (as if a dielectric panel were placed there to collect the plasma) instead than at the entrance, that is Eq. (16) was substituted by $\tilde{\boldsymbol{u}}_e(r, z_F) = \tilde{\boldsymbol{u}}_i(r, z_F)$. Results for this case, shown in Fig. 5, confirm the development of longitudinal electric currents, but now $\tilde{j}$

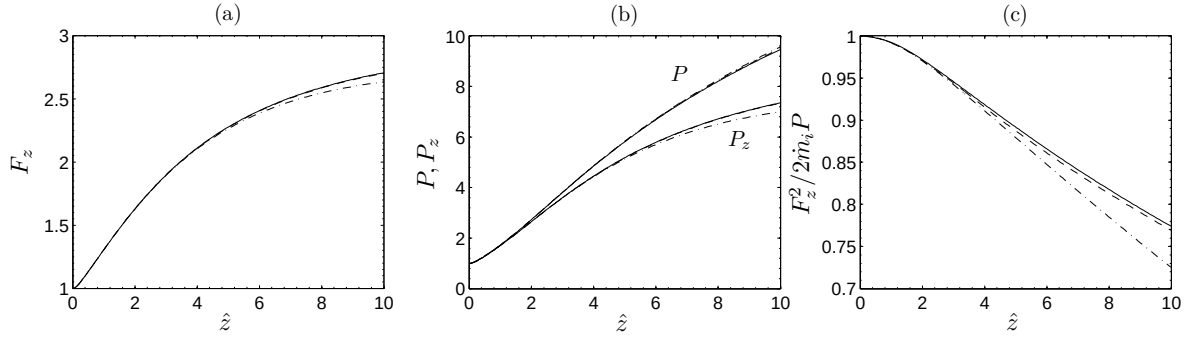

Figure 6. Axial evolution of ion (a) thrust, (b) axial and total power, and (c) acceleration efficiency, for $\hat{\Omega}_{i0} = 0.1$(solid), 10(dashed), and 100(dash-and-dot).

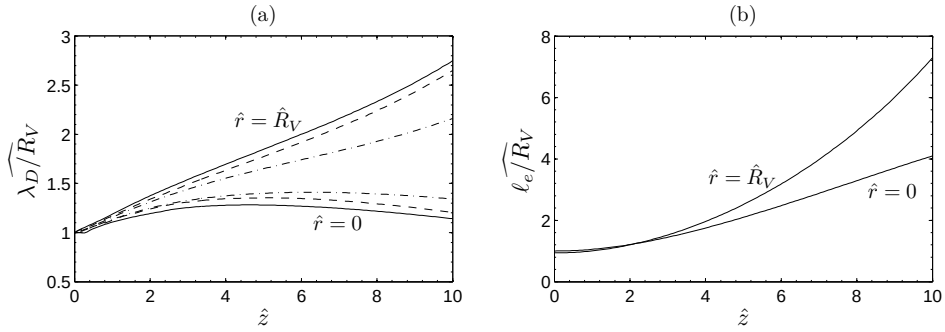

Figure 7. Evolution along the nozzle of the relative (a) quasineutrality and (b) magnetization parameters, for $\hat{\Omega}_{i0}$ =0.1(solid), 10(dashed), and 100(dash-and-dot). The relative magnetization parameter is independent of $\hat{\Omega}_{i0}$.

is negative in the central part and positive near the jet external border.

Figures 6(a)-6(c) show the downstream evolution of axial momentum and energy flows for ions, and the subsequent acceleration efficiency. The steady increase of F_z indicates a continuous conversion of electron enthalpy into ion directed energy, suggesting that the zero-enthalpy condition does not hold. The difference between P_z and P measures the radial energy imparted to ions, which is useless for thrust. Since it is found that $F_z^2/2\dot{m}_i P_z \approx 1$, the decrease in η_{noz} is due almost exclusively to the ion radial energy. In other words, $\eta_{noz} \approx P_z/P$. This behavior justifies also that efficiency is higher in the ion low-magnetization range, when the ion radial drift is smaller.

A. Evaluation of model assumptions

Two basic assumptions of the model are (1) plasma quasineutrality and (2) magnetic guiding of the electrons. They rely on λ_D/R_V and ℓ_e/R_V being small. Figures 7(a) and 7(b) plot the evolution of these two ratios along the nozzle; $\widehat{\lambda_D/R_V}$ and $\widehat{\ell_e/R_V}$ mean that values are given relative to $\lambda_D(0,0)/R$ and $\ell_e(0,0)/R$, respectively (equal to $2.4 \cdot 10^{-3}$ and $7.5 \cdot 10^{-3}$, respectively, for the case of Table 1). It is seen that the Debye-length ratio increases very slowly along the nozzle whereas the gyroradius ratio increases moderately. For the case of Table 1, where the two ratios are smaller than 10^{-2} at the entrance, plasma quasineutrality

and magnetic guiding of electrons are well preserved along the whole nozzle. Observe that $\ell_i/\ell_e = \sqrt{m_i/m_e}$ so that the relative change of ℓ_e/R_V coincides with that of ℓ_i/R_V; one has $\ell_i(0,0)/R = 2$ in Table 1.

Another basic assumption of the model was a negligible induced magnetic field, $\boldsymbol{B}'$. Once the electric current density is known, that field is computed from $\nabla \times \boldsymbol{B}' = \mu_0 \boldsymbol{j}$. The most interesting contribution is that of j_θ which induces a longitudinal field that stretches the streamlines of the applied-plus-induced magnetic field, favoring both the nozzle efficiency and the detachment.[12] In the case of a uniform jet with no Hall current, one has $j_{\theta e} = 0$ and $j_{\theta i} \ll \tilde{j}_i$, so that the longitudinal induced field is totally negligible.

IV. Conclusions

An axisymmetric model for the dynamics of a plasma jet in a divergent magnetic nozzle has been considered in the magnetically-guided limit for electrons. Ions, which are assumed cold, gain directed kinetic energy from conversion of electron thermal pressure, via an electrostatic self-field. For the isothermal electron population considered here pressure effects do not tend to zero and thus cannot be ignored downstream. Thrust, based on the ion momentum flow, and nozzle efficiency, based on the total kinetic power transmitted to ions, were determined.

Ion magnetization effects are found small except for extraordinarily high magnetic fields. The azimuthal ion current (i.e. plasma swirling) is always small. Simulations here were limited to the case of a uniform plasma jet at the entrance with no Hall current (i.e. zero azimuthal electron current). Then, no Hall current develops along the nozzle and the longitudinal induced magnetic field is negligible.

Simulations were run for a current-free plasma, satisfying the local ambipolarity condition, $\tilde{\boldsymbol{j}}(r,z) = 0$, at the nozzle entrance. In spite of this initial condition, the local ambipolarity condition, which constitutes a central assumption in the magnetic detachment model of Hooper, is not longer satisfied downstream. Indeed, there is a double failure of that condition, First, it is found that, except that for extremely high magnetic fields, ion streamsurfaces do not coincide with electron/magnetic streamsurfaces. Surface misalignment increases downstream of the nozzle. Although the misalignment angle seems modest, it is enough to lead to significantly different radial profiles of the ion and electron current densities at sections $z = \text{const}$. Ion and electron current densities can differ locally by a 100%. Compared to the electron flux, the ion flux is more focused around the jet axis.

We are now completing simulations for a plasma jet with a dominant contribution of the Hall current,[16] a case that matches better with plasma models upstream of the nozzle throat, presents richer dynamics, and can induce a longitudinal magnetic field. Analysis with more elaborate models for the electron distribution function are in progress. Also, the present model should be extended without much difficulty to ion populations with a high internal energy, relevant for some plasma thrusters.[3]

Acknowledgements

We thank Dr. Parra and Prof. Martínez-Sánchez for insightful and motivating discussions. This work was supported by the Ministerio de Ciencia e Innovación of Spain (Project ESP2007-62694) and the European Community (Grant 218862).

References

[1] G. Krülle, M. Auweter-Kurtz, and A. Sasoh, J. Propulsion and Power **14**, 754 (1998).

[2] S. A. Cohen, X. Sun, N. Ferraro, E. E. Scime, M. Miah, S. Stange, N. Siefert, and R. Boivin, IEEE Transactions on Plasma Science **34**, 792 (2006).

[3] A. Arefiev and B. Breizman, Physics of Plasmas **11**, 2942 (2004).

[4] D. Courtney and M. Martínez-Sánchez, Diverging Cusped-Field Hall Thruster, in *30th International Electric Propulsion Conference, Florence, Italy*, IEPC-2007-39, Electric Rocket Propulsion Society, Fairview Park, OH, 2007.

[5] S. A. Andersen, V. O. Jensen, P. Nielsen, and N. D'Angelo, Phys. Fluids **12**, 557 (1969).

[6] C. A. Deline, R. D. Bengtson, B. N. Breizman, M. R. Tushentsov, J. E. Jones, D. G. Chavers, C. C. Dobson, and B. M. Schuettpelz, Physics of Plasmas **16**, 033502 (2009).

[7]E. B. Hooper, Journal of Propulsion and Power **9**, 757 (1993).

[8]A. Arefiev and B. Breizman, Physics of Plasmas **12**, 043504 (2005).

[9]B. N. Breizman, M. R. Tushentsov, and A. V. Arefiev, Physics of Plasmas **15**, 057103 (2008).

[10]E. Ahedo and M. Martínez-Sánchez, The Role Of Current-Free Double-Layers In Plasma Propulsion, in *44th Joint Propulsion Conference, Hartford, CT*, AIAA 2008-5005, American Institute of Aeronautics and Astronautics, Washington DC, 2008.

[11]C. Charles and R. Boswell, Applied Physics Letters **82**, 1356 (2003).

[12]R. Winglee, T. Ziemba, L. Giersch, J. Prager, J. Carscadden, and B. R. Roberson, Physics of Plasmas **14**, 063501 (2007).

[13]I. Mikellides, P. Mikellides, P. Turchi, and T. York, Journal of Propulsion and Power **18**, 152 (2002).

[14]M. Abramowitz and I. Stegun, *Handbook of Mathematical Functions*, Dover, New York, 1965.

[15]M. Zucrow and J. Hoffman, *Gas dynamics* , Wiley, New York, 1976.

[16]E. Ahedo and M. Merino, in *31th International Electric Propulsion Conference, Ann Arbor, Michigan, USA*, IEPC 2009-002, Electric Rocket Propulsion Society, Fairview Park, OH, 2009.